

In-plane Ising superconductivity revealed by exchange interactions

Junyi Yang^{1†}, Changjiang Liu^{1,2†}, Xianjing Zhou³, John Pearson^{1,3}, Alexey Suslov⁴, Dafei Jin^{3,5}, Jidong S. Jiang¹, Ulrich Welp¹, Michael R. Norman¹, Anand Bhattacharya^{1*}

1. Materials Science Division, Argonne National Laboratory, Lemont, USA
2. Department of Physics and Astronomy, University of Buffalo, Buffalo, USA
3. Center for Nanoscale Materials, Argonne National Laboratory, Lemont, USA
4. National High Field Magnetic Laboratory, Tallahassee, USA
5. University of Notre Dame, Notre Dame, USA

Abstract

Two-dimensional superconductors with spin-textured Fermi surfaces can be a platform for realizing unconventional pairing and are of substantial interest in the context of quantum information science, and superconducting spintronics/orbitronics. We find that the superconducting 2D electron gas (2DEG) formed at $\text{EuO}_x/\text{KTaO}_3$ (110) interfaces, where the EuO_x is magnetic, has a spin-texture with an unusual in-plane ‘Ising’ like uniaxial anisotropy that is revealed in measurements of the in-plane critical field in the superconducting state, as well as from quantum corrections to the magnetoresistance in the normal state. This spin texture is not evident in $\text{AlO}_x/\text{KTaO}_3$ (110) where the overlayer is non-magnetic. Our results are consistent with a highly anisotropic spin-textured Fermi surface in 2DEGs formed at the KTaO_3 (110) interface that is ‘hidden’ from external magnetic fields due to a near cancellation between orbital and spin moments but revealed by exchange interactions of the electrons in the 2DEG with Eu moments near the $\text{EuO}_x/\text{KTaO}_3$ (110) interface. Our findings demonstrate that magnetic overlayers provide a unique probe of spin textures and related phenomena in heterostructures.

†equal contribution

*anand@anl.gov

Introduction

The interplay of large spin-orbit coupling (SOC) with crystalline symmetry breaking can result in non-trivial spin-textures for electrons at the Fermi surface of a two-dimensional electron gas (2DEG). In superconducting 2DEGs, such spin textures can lead to an order parameter with a p -wave component,¹ which is of both fundamental interest² and also relevant for realizing fault tolerant qubits³, and novel forms of superconducting spintronics⁴ and orbitronics⁵ when coupled to magnetic layers. Recently, it was shown the presence of strong SOC with in-plane inversion symmetry breaking in a 2D superconductor can lock spins along the out-of-plane direction, resulting in a uniaxial ‘Ising’ spin-texture. This leads to highly anisotropic properties in the superconducting state with large in-plane critical fields^{6,7}, well in excess of the Pauli limit. We note that there is also ‘type-II’ Ising superconductivity, without inversion symmetry breaking⁸. On the other hand, out-of-plane inversion symmetry breaking can lead to a ‘Rashba’ spin texture, where spins are locked in-plane with opposite helicity on spin-split Fermi surfaces⁹. However, direct experimental evidence for the role of spin textures in the properties of 2D superconductors, and their coupling to magnetism, is not well established. Here we present evidence for a new kind of spin texture in a superconducting 2DEGs – an ‘in-plane Ising’ spin texture, with a strong uniaxial in-plane anisotropy, revealed by an anisotropic exchange interaction between the electrons in the 2DEG and a ferromagnetic overlayer.

Superconductivity was recently discovered in 2DEGs formed at interfaces of KTaO_3 (KTO)¹⁰. Notably, the T_c in KTO 2DEGs was found to strongly depend on the orientation of the interface¹⁰⁻¹² and it was proposed that the orientation dependence of T_c is due to varying levels of degeneracy in the t_{2g} manifold of the Ta- $5d$ bands in quantum-confined 2DEGs formed on different crystalline facets of KTO¹². For the KTO (110) interface (Fig. 1(a)), the degenerate d_{xz}/d_{yz} states at the Γ point are lower in energy than d_{xy} due to confinement along the [110] axis and they form an anisotropic Fermi surface with larger/smaller effective mass along the $[1\bar{1}0]/[001]$ axis¹³, respectively. Furthermore, the d_{xz}/d_{yz} states at Γ form the combination $d_{yz} \pm id_{xz}$ with an orbital angular momentum axis oriented along the in-plane [001] direction. Due to SOC, the spins anti-align to these orbital moments, and this gives rise to an in-plane ‘Ising’ like anisotropy for both orbital and spin textures along [001] with no spin canting along the out-of-plane direction. Additionally, broken inversion symmetry at the KTO (110) interface gives rise to Rashba splitting of bands formed from these states, which along with the Ising-like anisotropy

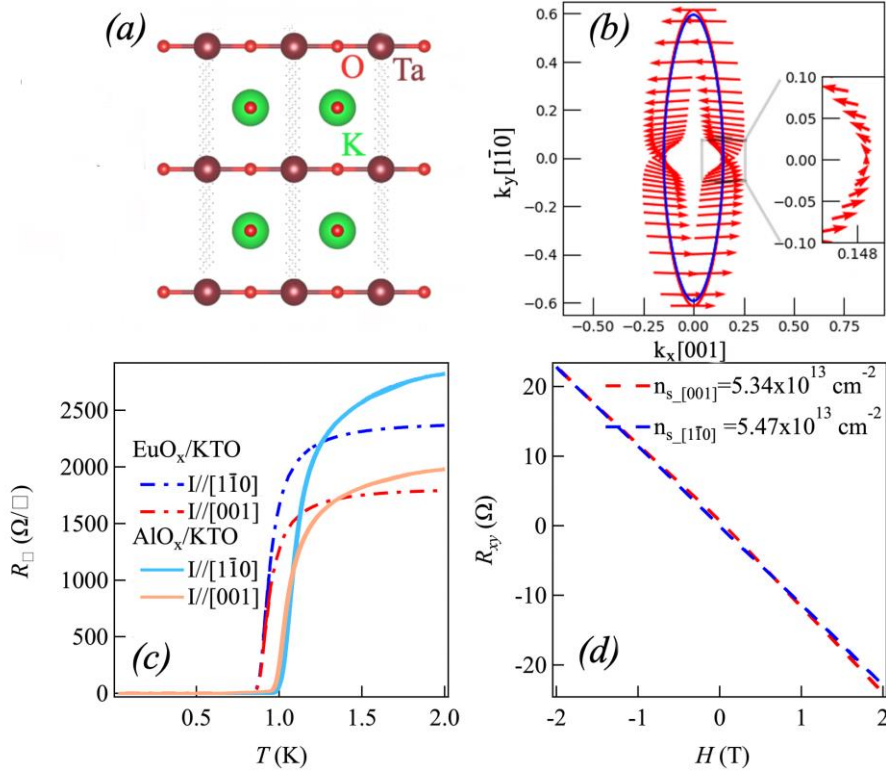


Figure 1. (a) Schematic diagram of the KTO (110) lattice. (b) KTO (110) Fermi surface with its anisotropic spin texture. The length of the arrows is related to the spin vector size, with the inset showing an expanded view around [001]. The two Rashba split surfaces are shown in red and blue, but the spin texture of only one of them is presented for clarity. (c) Temperature dependence of the sheet resistance of EuO_x/KTO and AlO_x/KTO with current applied along two different in-plane directions. The light blue solid line denotes the current along $[1\bar{1}0]$ and the light red solid line denotes the current along $[001]$ for AlO_x/KTO . The blue dashed line denotes the current along $[1\bar{1}0]$ and the red dashed line denotes the current along $[001]$ for EuO_x/KTO . (d) Hall measurements for Hall bar devices along the $[001]/[1\bar{1}0]$ directions, respectively.

induces a dominant $\mathbf{k}_y \hat{\sigma}_x$ texture due to spin-momentum locking (here x refers to $[001]$ and y to $[1\bar{1}0]$) (Fig. 1(b)). The ‘anti-alignment’ of orbital and spin moments also leads to a strongly reduced g -factor for single electron occupancy in the t_{2g} manifold^{14,15}, and a reduced Zeeman coupling of external magnetic fields to the electronic spin texture.

Results

In this work we report on an Ising-like in-plane spin texture for KTO_3 (110) interfaces which is revealed by the anisotropy of the in-plane H_c as well as the normal state magnetoresistance for EuO_x/KTO (110) 2DEGs, where the EuO_x overlayer is magnetic. We fabricated Hall bar devices

on both $\text{AlO}_x/\text{KTO}(110)$ and $\text{EuO}_x/\text{KTO}(110)$ (Fig. S1) 2DEGs. Here AlO_x is non-magnetic, while EuO_x is ferromagnetic with $T_{\text{Curie}} \sim 70$ K. Figure 1(c) shows the temperature dependence of the sheet resistance (R_{\square}) for both AlO_x/KTO and EuO_x/KTO with current along $[001]/[1\bar{1}0]$, respectively. The crystallographic axis for each direction is resolved through x-ray diffraction (Fig. S2). Superconductivity with vanishingly small resistance is observed for both samples below 800 mK. The normal state R_{\square} for a current along $[1\bar{1}0]$ is observed to be larger than that for a current along $[001]$ by a factor of 1.5 for all samples. These observations are consistent with a highly anisotropic Fermi surface of KTO (110)¹³ (Fig. 1(b)), where the effective mass along the $[1\bar{1}0]$ direction is larger than that along $[001]$. Hall measurements (Fig. 1(d)) along these two crystallographic directions are nearly identical, and the anisotropic R_{\square} is then due to the anisotropy in electron mobility. We note that for LAO/STO (110), a similar anisotropy in R_{\square} is observed, but that changes as a function of carrier density¹⁶⁻¹⁸ due to occupation of the d_{xy} bands at higher densities. In the present study, the anisotropy of the normal state R_{\square} is similar for both low and high densities. This may imply that the d_{xy} bands are not occupied in our KTO (110) 2DEGs, presumably due to the stronger confinement effects in KTO (110) relative to STO (110). However, we note that recent angle-resolved photoemission experiments at a higher density do observe the occupation of the higher lying d_{xy} bands in doped KTO (110)¹³ surfaces.

Anisotropic Superconductivity

To explore the anisotropic spin-texture and superconductivity in KTO (110) 2DEGs, we measured the dependence of T_c on in-plane magnetic fields along $[001]$ and $[1\bar{1}0]$ for AlO_x/KTO samples (Figure 2(a)-(b)). At all temperatures, superconductivity is suppressed more rapidly for fields along $[1\bar{1}0]$. Figure 2(c) summarizes the T_c dependence of H_c for the $[001]$ and $[1\bar{1}0]$ directions. T_c is taken as the inflection point in the temperature dependence of R_s and is normalized to its zero field value and H_c is normalized to the Pauli paramagnetic¹⁹ field H_p . A square-root like H_c vs T_c is consistent with Ginzburg-Landau (GL) theory for a 2D superconductor²⁰. $H_c/[001]$ is only slightly (< 2%) larger than $H_c/[1\bar{1}0]$ near T_c , but the difference is as high as 25% at the lowest temperatures measured. The same anisotropy is found in a lower T_c sample (Fig. S3). We also rotate the magnetic field in-plane (Figure 2(d)) to obtain the full angular dependence of the in-plane H_c at $T \lesssim T_c$. The angular dependence of the sheet resistance normalized to that along $[001]$ ($R_{\text{ANI}} = R(\varphi) / R(H//[001])$) shows a slightly elliptical shape.

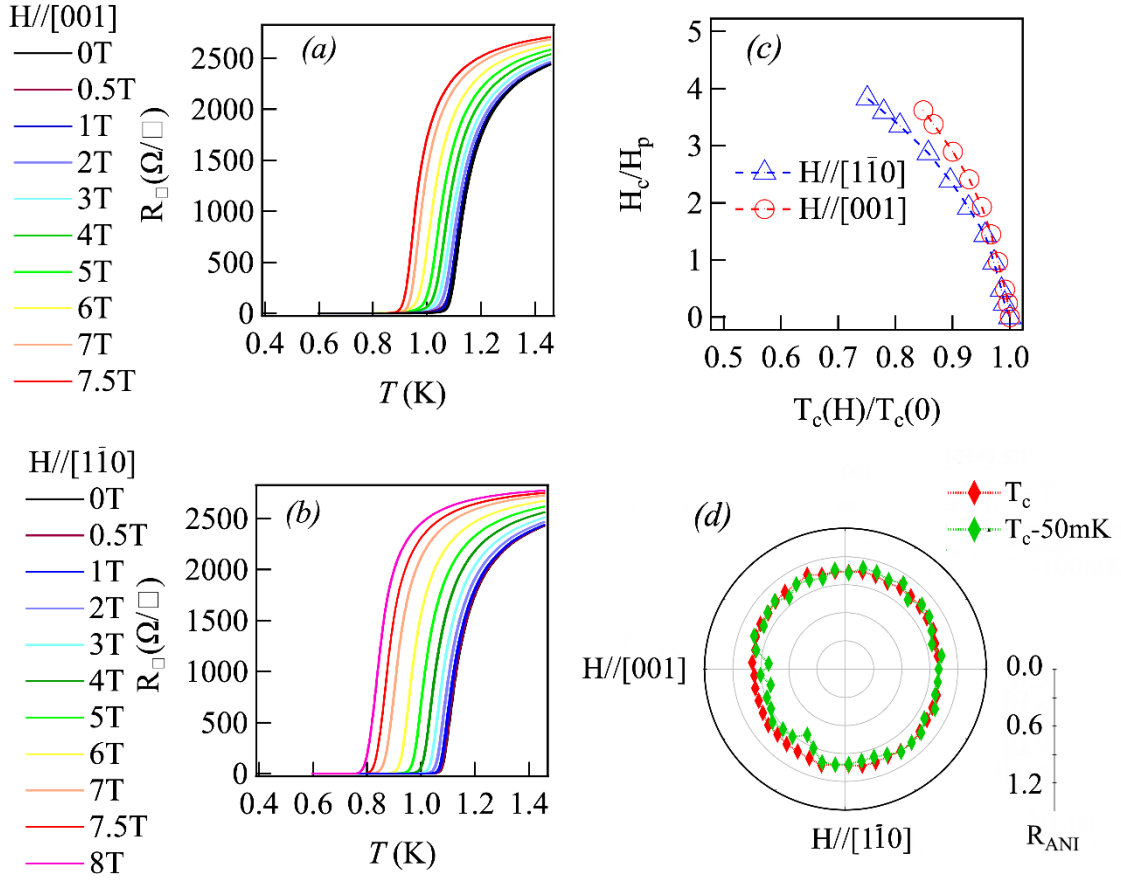


Figure 2. Temperature dependence of the sheet resistance of AlO_x/KTO for different in-plane fields when (a) the field is applied along $[001]$ and (b) when the field is applied along $[1\bar{1}0]$. (c) Temperature dependence of the critical field of AlO_x/KTO for the $[1\bar{1}0]$ and $[001]$ field directions. T_c is normalized to its zero-field value and H_c is normalized to the Pauli paramagnetic field. (d) The angular dependence with respect to the field direction of the normalized sheet resistance for AlO_x/KTO with a field of 0.5 T at two different temperatures.

Despite the highly anisotropic spin-texture anticipated for KTO (110) 2DEGs, the anisotropy observed in AlO_x/KTO is likely due to the anisotropy of the orbital-limiting field. From a single band GL model, the ratio of the orbital critical field along the two directions is approximately related to the inverse ratio of the effective masses. Our resistance measurements in the normal state are consistent with an effective mass $m_{[1\bar{1}0]} > m_{[001]}$, resulting in $H_c/[001] > H_c/[1\bar{1}0]$ as observed. Both spin-orbit scattering, and the reduced g -factor, would play a role in increasing the paramagnetic limiting field to higher values^{21,22}. Fits of the critical field using Werthamer-Helfand-

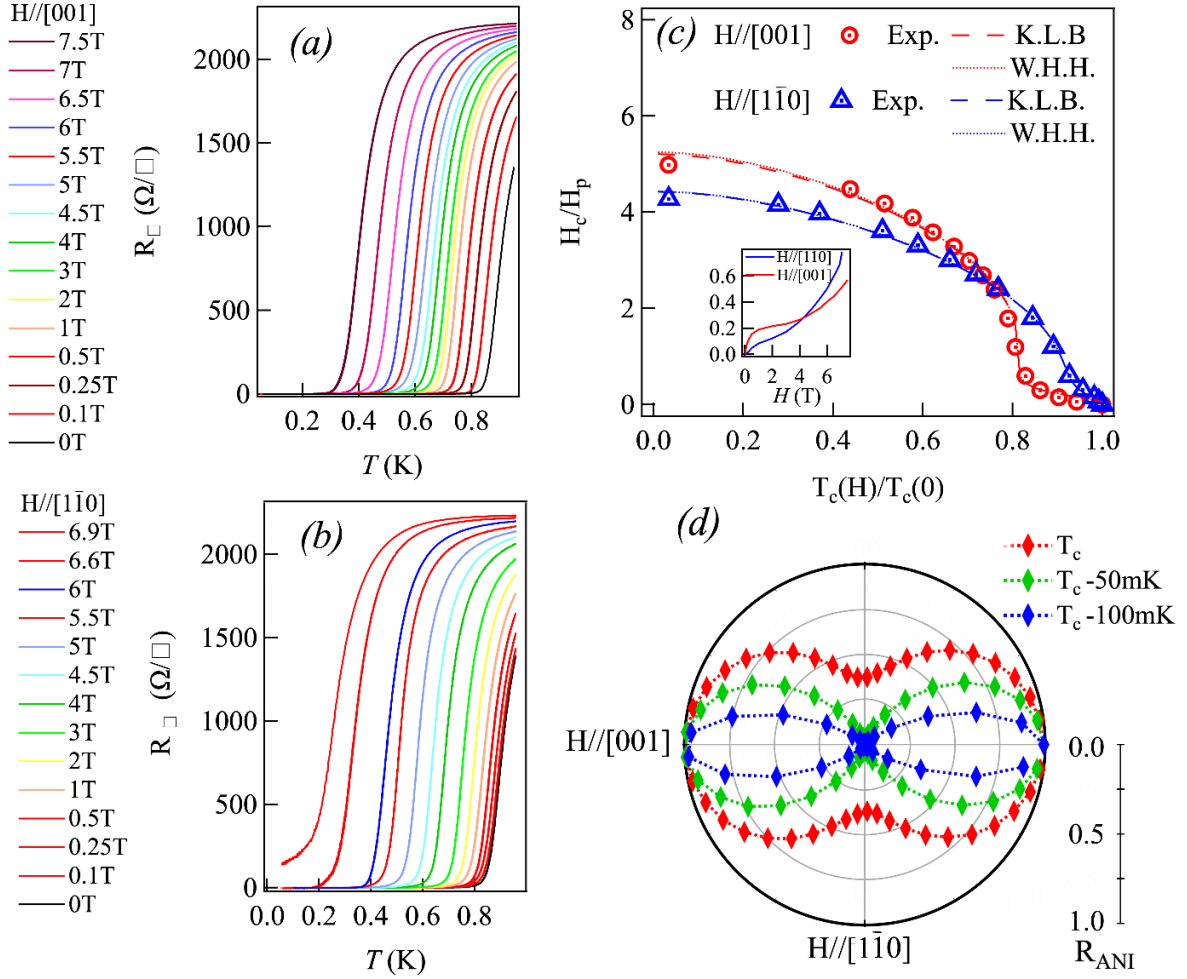


Figure 3. Temperature dependence of the sheet resistance of EuO_x/KTO for different in-plane fields when (a) the field is applied along $[001]$ and (b) when the field is applied along $[1\bar{1}0]$. (c) Temperature dependence of the critical field of EuO_x/KTO for the $[1\bar{1}0]$ and $[001]$ field directions. T_c is normalized to its zero-field value and H_c is normalized to the Pauli paramagnetic field. The solid/dashed line denotes fits based on the KLB/WHH models described in the text. The inset shows the KLB pair-breaking parameter, $\alpha(h)$. (d) The angular dependence of the normalized sheet resistance of EuO_x/KTO for an in-plane field of 0.5 T for three different temperatures.

Hohenberg (WHH)²³ theory for a lower T_c sample with a wider dynamic range in temperature are consistent with a reduced g -factor (S13). While effective mass anisotropy is temperature independent, a finite g -factor and anisotropic spin-orbit scattering can result in a modest variation of the anisotropy as a function of temperature (S13).

Figure 3(a)-(b) shows the temperature dependence of R_{\square} of EuO_x/KTO (110) when the field is applied along the [001] and $[1\bar{1}0]$ directions. H_c along [001] and $[1\bar{1}0]$ is also determined from the field dependence of R_{\square} at 23 mK (Fig S4). $H_c//[1\bar{1}0]$ is smaller than $H_c//[001]$ at the lowest temperatures; however, at higher temperatures close to T_c , the relation is reversed. Figure 3(c) summarizes the T_c dependence of H_c for both directions. $H_c//[001]/H_c//[1\bar{1}0] \sim 1.20$ at the lowest temperatures in EuO_x/KTO (110), consistent with AlO_x/KTO (110). However, closer to T_c , the ratio *inverts* and $H_c//[001]/H_c//[1\bar{1}0] < 0.1$ for EuO_x/KTO (110). This anisotropy switching in H_c is also observed in EuO_x/KTO samples with different T_c (Figs. S5-7). The anisotropic H_c close to T_c is evident in the angular dependence of the normalized R_{\square} (or R_{ANI}) under a 0.5 T in-plane magnetic field (Fig. 3(d)). A dumbbell-shaped angular dependence is observed with a minimum of R_{ANI} for a magnetic field along $[1\bar{1}0]$, namely $H_c//[1\bar{1}0] > H_c//[001]$. We note that the out-of-plane $H_c//[110]$ is consistent with other reports (Fig. S8).

Our data are reminiscent of Chevrel phase superconductors like EuMo_6S_6 where an internal field due to the presence of local moments has a profound impact on H_c and can give rise to an inflection-like behavior near T_c ²⁴. We suggest a scenario involving the interaction of the spins of the Eu ‘impurity’ ions, which diffuse into KTO, with the anisotropic spin texture of the KTO (110) 2DEG^{10,25,26}. The external field rapidly polarizes the Eu spins, and they in turn interact with electrons at the Fermi surface via an exchange interaction. This gives rise to an extra pair-breaking term that acts to suppress H_c for temperatures near T_c , that follows the polarization of the Eu moments. We note that the pure Zeeman term couples the external magnetic field with the total moment of the electron, and not just the spin. Due to the suppression of the g -factor in KTO (110) 2DEGs, this coupling is strongly reduced. On the other hand, the exchange interaction to lowest order involves the electron spin only, and thus remains significant.

To illustrate this, we generalize an approximate formula given by Klemm, Luther and Beasley (KLB)²⁷ by including an exchange field in their pair-breaking function $\alpha(h)$ that determines H_c :

$$\ln(t) = \psi\left(\frac{1}{2}\right) - \psi\left(\frac{1}{2} + \frac{\alpha(h)}{2\pi k_B T}\right) \quad (1)$$

where ψ is the digamma function, t is the reduced temperature (T/T_c), and h , the reduced field, enters $\alpha(h)$ as h^2 as we are considering in-plane fields.

$$\alpha(h) = ch^2 + \frac{1}{2b} \left(\frac{g}{2} h + h_J \right)^2 \quad (2)$$

where c is πT_c , b^{-1} is $3\tau_{\text{so}}$ with τ_{so} the spin-orbit scattering time, and h_J is the reduced exchange field between the paramagnetic Eu impurity ions ($J = 7/2$) and the tantalum conduction electrons which is described by a Brillouin function $h_J = h_{J0} B_J(Jg'\mu_B H/k_B T)^{30}$ ($g' = 2$). Since the spin texture in Fig. 1(b) has an ‘Ising’ like in-plane anisotropy, h_J is larger for fields along [001] compared to fields along $[1\bar{1}0]$. Thus, when the external field is applied along the [001] direction, the pair-breaking function $\alpha(h)$ will rapidly increase at small fields following the H/T dependence of the Brillouin function. Due to this ‘boost’ to $\alpha(h)$ provided by the exchange field, the required external field for pair-breaking is greatly reduced, and $H_c/[001]$ is much smaller for T near T_c . Once the moment is saturated, the relative contribution of the ‘exchange’ term is diminished as the field increases further, and at the lowest temperatures H_c vs T_c is dominated by pair-breaking due to orbital effects. Therefore, both EuO_x/KTO and AlO_x/KTO show similar behavior at low T . We extract $\alpha(h)$ from our experimental H_c and fit it using Eq. (2) assuming $g = 0.5$ (S13) and find that $\frac{h_J[001]}{h_J[1\bar{1}0]} \sim 1.33$. An alternative fit to the data can be done by using an in-plane formula for H_c which is based on WHH supplemented by the exchange field²⁸ (S13). As with the KLB fit, the exchange field has a negative sign with respect to applied field in the WHH fit, and a similar ratio of $\frac{h_J[001]}{h_J[1\bar{1}0]} \sim 1.29$ is obtained. While a non-zero g -factor implies a Zeeman contribution to pair-breaking from the applied field, the exchange field remains the dominant pair-breaking factor near T_c .

For context, the crossover in the anisotropy in H_c has been observed²⁹⁻³¹ in a quasi-1D superconductor $\text{K}_2\text{Cr}_3\text{As}_3$, which arises from an anisotropic spin susceptibility along and perpendicular to its 1D chains, though these data do not show the pronounced inflection in $H_c(T_c)$ we see for fields along [001] in EuO_x/KTO (110). Notably, measurements of the Knight shift in $\text{K}_2\text{Cr}_3\text{As}_3$ in the superconducting state suggest a triplet component³². Two-fold modulations of the in-plane H_c have also been observed in several 2D superconductors, and have been attributed to emergent nematicity,³³ and mixing of s -wave with d -wave or p -wave order parameters^{34,35}. While a Lorentz force resulting from magnetic fields could lead to a two-fold symmetry of the in-plane H_c if vortices move freely, the observed results in EuO_x/KTO are independent of the current direction (Fig. S9). More recently, two-fold H_c modulations have been ascribed to anisotropic spin susceptibilities that result from 3D spin textures of the Fermi surface due to broken mirror

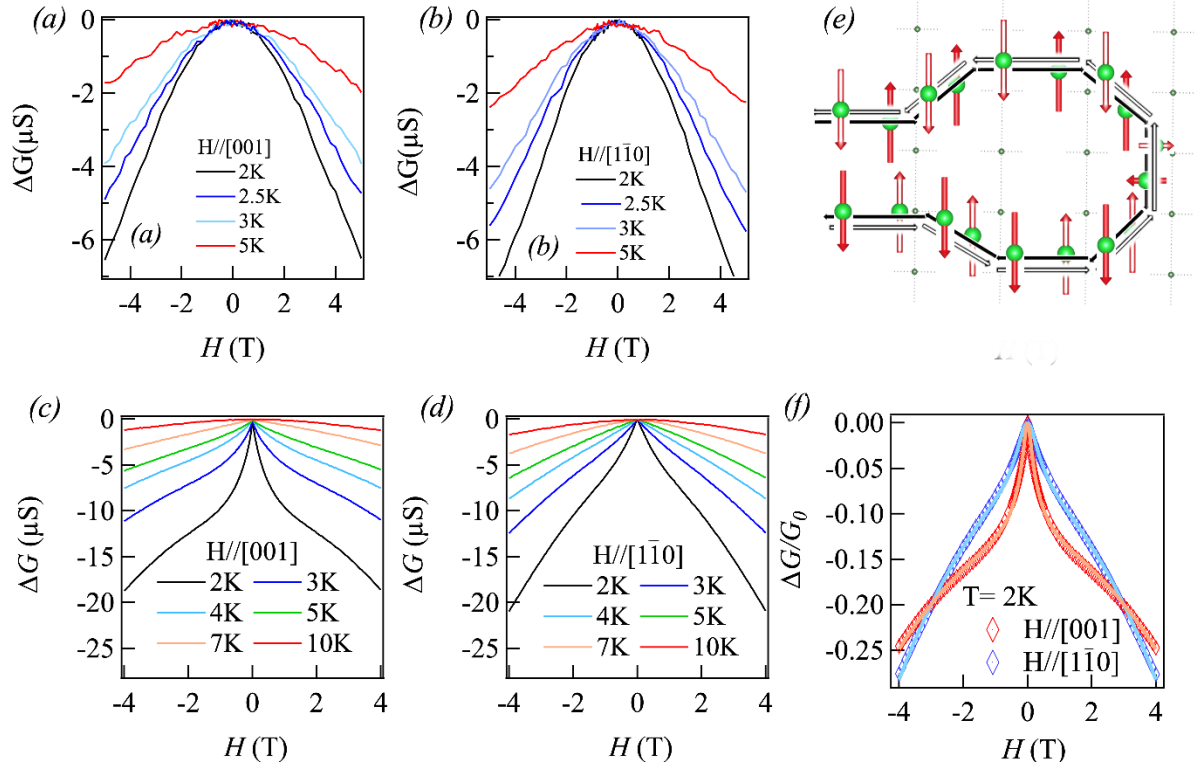


Figure 4. Field dependence of the magnetoconductance at different temperatures for AlO_x/KTO for an in-plane magnetic field applied (a) along the $[001]$ direction and (b) along the $[1\bar{1}0]$ direction. (c) and (d) are the same as (a) and (b) but for EuO_x/KTO . (e) Schematic of the destructive interference for an electron scattering in time-reversed closed loop paths in $\text{KTO}(110)$ with spins (shown by solid and hollow red arrows) locked along the $[001]$ axis. (f) Weak anti-localization fits to the magnetoconductance of EuO_x/KTO at 2 K for both in-plane field directions as described in the text.

symmetries, and the interplay of parity with spin-orbit coupling near band-inversion points in reciprocal space³⁶⁻³⁸. However, experimental evidence for these spin textures in the normal state is not well established.

Anisotropic Magnetotransport

To further investigate the anisotropic spin-texture in $\text{KTO}(110)$ 2DEGs, we carried out low-temperature magnetoconductance measurements in the normal state. Quantum interference of conduction electrons in the presence of SOC results in a positive magnetoresistance known as weak anti-localization (WAL). WAL for an out-of-plane field has been observed for 2DEGs in both $\text{KTO}(111)$ and $\text{KTO}(110)$ ³⁹⁻⁴¹. In 2DEGs formed at the $\text{NdTiO}_3/\text{SrTiO}_3$ interface, it was shown

that exchange coupling due to local magnetic moments can enhance the dephasing of electrons under *in-plane* fields,⁴² and thus WAL effects in this geometry can probe the in-plane spin susceptibility. Thus, we first measured the magnetoconductance in AlO_x/KTO (110) at different temperatures for in-plane fields along [1 $\bar{1}$ 0] and [001] (Fig. 4(a)-(c)). A broad quadratic field dependence of the magnetoconductance is observed along both directions, with a decrease in the magnetoconductance as the temperature increases due to the loss of phase coherence in the field. A cusp-like behavior is only observed for fields along the out-of-plane direction (Fig. S10). This mirrors what occurs for H_c , where the orbital field enters linearly in H for perpendicular fields but quadratic in H for parallel fields, given that the Cooperon that is associated with WAL has similar properties to the Cooper pair propagator for superconductivity. Figure 4(c)-(d) shows the magnetoconductance measured on EuO_x/KTO (110) at different temperatures for the two in-plane field directions. In strong contrast to AlO_x/KTO (110), a sharp cusp in the field dependence of the magnetoconductance is observed when the field is applied along [001]. As the temperature increases from 2 K, the cusp feature is attenuated and the magnetoconductance decreases sharply as quantum corrections are lost. For fields applied along [1 $\bar{1}$ 0], a noticeably broader cusp-like feature is observed at 2 K, but with a similar temperature dependence as for [001]. Since the orbital corrections to the magnetoconductance should be quadratic and small for in-plane fields in a quasi-2D limit, we look to the Zeeman contribution²⁹ to the dephasing of WAL in the magnetoconductance,^{42,31}

$$\Delta G(H_{//}) = -\frac{G_0}{2} \ln \left(1 + \frac{\Delta_\Phi(H_{//})}{B_\Phi} \right) \quad (3)$$

where $\Delta_\Phi(H_{//}) = \frac{[2\mu_B(H_{//})]^2}{(4eD)^2 B_{so}}$. Here, D is the diffusion constant, B_{so} is the field scale associated with spin-orbit scattering, B_Φ is the orbital dephasing field scale, and G_0 is the quantum of conductance. For an in-plane field H , this gives rise to a quadratic field dependence. However, as with H_c , for EuO_x/KTO, we expect that the Eu impurity moments in the KTO 2DEGs will induce an additional exchange term that will sharply enhance the effective field that enters into the Zeeman term⁴³ $H_{//} = \frac{g}{2}H + H_J$. The first term in $H_{//}$ is small since g is strongly reduced due to quenching of the total moment, and the field-induced dephasing is dominated by the exchange interaction between Eu moments and the ‘in-plane Ising’ spin polarized electrons (Fig. 4(e)). At low temperatures, the Eu moments align rapidly with H leading to the pronounced ‘boost’ in the

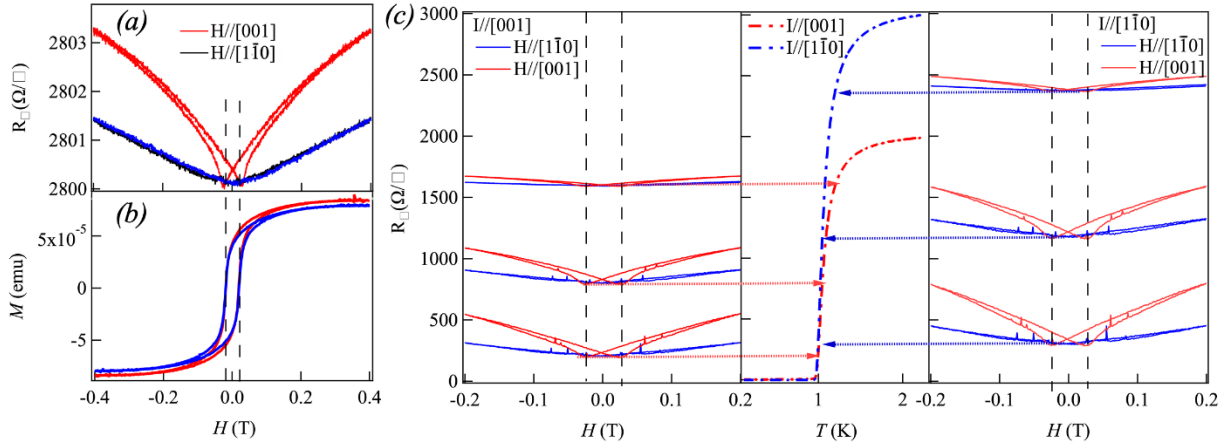


Figure 5 (a) Field dependence of the sheet resistance for EuO/KTO(110) at 2 K. The red solid line denotes a field along [001] and the blue solid line denotes a field along $[1\bar{1}0]$. (b) Field dependence of the magnetic moment for EuO/KTO(110) at 2 K, showing a nearly isotropic coercivity. The red solid line denotes a field along [001] and the blue solid line denotes a field along $[1\bar{1}0]$. (c) Field dependence of the sheet resistance for EuO/KTO (110) with current applied along different crystal axes. The left panel shows the field dependence of the sheet resistance when the current is applied along [001]. The right panel shows the field dependence of the sheet resistance when the current is applied along $[1\bar{1}0]$. The red solid line denotes a field along [001] and the blue solid line denotes a field along $[1\bar{1}0]$. The central panel shows the temperature dependence of the sheet resistance for $I//[001]$ (red solid dashed line) and $I//[1\bar{1}0]$ (blue solid dashed line). The arrows are used to indicate the different temperatures that the field dependence of the resistance is taken at.

exchange interaction at low fields with electrons in the KTO 2DEGs, and a quasi-linear behavior is seen in the magnetoconductance. At higher fields, the impurity moments saturate, and we anticipate crossing over to a quadratic behavior as expected from orbital contributions. We thus fit our data using Eq. 3 with the same g and the same exchange field as in our H_c analysis (See SI Table 2). These fits are excellent indicating that our H_c and magneto-resistance (MR) analysis are consistent with one another.

In addition to the WAL correction to the MR, a hysteretic MR has been observed in 2DEGs formed at $\text{LaAlO}_3/\text{SrTiO}_3$, $\text{GdTiO}_3/\text{SrTiO}_3$ and $\text{LaTiO}_3/\text{SrTiO}_3$ interfaces when magnetism is induced⁴⁴⁻⁴⁶. Recent work also shows hysteretic MR at KTO interfaces^{47,48} (though we do not observe the in-plane anisotropy of T_c claimed in Ref. 47). For EuO_x/KTO , we observed a weak anomaly in the MR of $\sim 0.1\%$ near the Curie temperature of the EuO_x overlayer indicating an interfacial coupling

or scattering between the EuO_x and the 2DEGs (Fig. S11). We then measured the low-field MR at 2 K, and a clear hysteretic behavior is observed at low fields in the MR for $H // [001]$ (Fig. 5(a)). The hysteretic minima in the MR differ by 230 Oe, consistent with the in-plane coercive field of the EuO_x overlayer of ~ 115 Oe for this sample (Fig. 5(b)) and it persists from 2 K down to T_c (Fig. 5(c)). Notably, the effect is strongly anisotropic - the MR for $H // [001]$ is larger than that for $H // [1\bar{1}0]$, while being similar for current directions along $[001]$ and $[1\bar{1}0]$. This is again consistent with an in-plane Ising spin texture. We note that the coercive field of EuO_x varies due to different sample growth conditions and aging effects.

We consider several mechanisms for the hysteretic MR in EuO_x/KTO (110) near T_c . We rule out spin-flip scattering for electrons in the 2DEG from magnetic domains in EuO_x , since that gives rise to a negative MR at high fields⁴⁹. An alternative mechanism based on the Lorenz force would give rise to a positive MR⁵⁰, though we note that by this mechanism when we change the direction of current from $[001]$ to $[1\bar{1}0]$, that would change the nominal velocity due to differences in the effective mass, and thus also the MR. However, we observe that the anisotropy of the MR only depends on the direction of H relative to the crystal lattice and is much less dependent on the direction of the current, which would argue against an effect based on the Lorenz force. The significant increase in the MR near the superconducting transition in Fig. 5 (c) suggests a pair-breaking effect. We propose that this pair-breaking arises from exchange coupling of ferromagnetic Eu spins in EuO_x to the 2DEGs, with anisotropy arising from the in-plane Ising spin texture of the 2DEGs. We also note that the pair-breaking of ferromagnetic Eu spins in EuO_x is relatively weak, and only clearly observable near T_c . At lower temperatures, as the amplitude of the superconducting order parameter grows, there are no signatures of the effects of ferromagnetic EuO_x .

Summary

In summary, we presented evidence for an in-plane Ising-like spin texture in KTO (110) 2DEGs. The texture is ‘hidden’ in applied magnetic fields in AlO_x/KTO , presumably due to a strongly reduced g -factor, but for EuO_x/KTO the presence of an exchange field from the Eu ions ‘lights up’ the Ta-5d spin texture and allows us to see its consequences for both the critical field in the superconducting state as well the low-temperature normal state magnetoconductance. In addition to revealing the spin texture at KTO (110) interfaces, the magnetic proximity effects offer a path

to control superconductivity, which can be further explored by using different magnetic overlayers in future studies of these heterostructures. The unique in-plane Ising ($\mathbf{k}_y \hat{\sigma}_x$) nature of the spin texture intrinsic to all KTO (110) 2DEGs may have consequences both for the nature of superconductivity in these 2DEGs and for possible applications. In particular, the triplet component of the Cooper pairs that can be admixed in due to inversion breaking should exhibit the same in-plane Ising anisotropy as we find here.

Acknowledgements:

We thank Ivar Martin for discussions. All research presented here is supported by the Materials Science and Engineering Division, Office of Basic Energy Sciences, U.S. Department of Energy. The use of facilities at the Center for Nanoscale Materials was supported by the U.S. DOE, BES under Contract No. DE-AC02-06CH11357. C.L. acknowledges partial financial support from the College of Arts and Sciences, University at Buffalo, SUNY.

Contributions:

Synthesis of samples was carried out by J.Y. and C.L. with assistance from A.B. and J.P. All low-temperature magneto-transport and magnetization measurements were carried out by J.Y. and C.L. with assistance from U.W., A.S., J.S.J., X.J. and D.J. The theory analysis presented here was carried out by M.R.N. along with J.Y. and A.B. The paper was written by J.Y., M.R.N. and A.B. and all authors contributed to discussions regarding the paper.

References

- 1 Smidman, M., Salamon, M. B., Yuan, H. Q. & Agterberg, D. F. Superconductivity and spin-orbit coupling in non-centrosymmetric materials: a review. *Reports on Progress in Physics* **80**, 036501, doi:10.1088/1361-6633/80/3/036501 (2017).
- 2 Frolov, S. M., Manfra, M. J. & Sau, J. D. Topological superconductivity in hybrid devices. *Nature Physics* **16**, 718-724, doi:10.1038/s41567-020-0925-6 (2020).
- 3 Desjardins, M. M. *et al.* Synthetic spin-orbit interaction for Majorana devices. *Nature Materials* **18**, 1060-1064, doi:10.1038/s41563-019-0457-6 (2019).
- 4 Linder, J. & Robinson, J. W. A. Superconducting spintronics. *Nature Physics* **11**, 307-315, doi:10.1038/Nphys3242 (2015).

- 5 Amundsen, M., Linder, J., Robinson, J. W. A., Zutic, I. & Banerjee, N. Spin-orbit effects in superconducting hybrid structures. *Rev Mod Phys* **96**, 021003, doi:10.1103/RevModPhys.96.021003 (2024).
- 6 Lu, J. M. *et al.* Evidence for two-dimensional Ising superconductivity in gated MoS₂. *Science* **350**, 1353-1357, doi:10.1126/science.aab2277 (2015).
- 7 Saito, Y. *et al.* Superconductivity protected by spin–valley locking in ion-gated MoS₂. *Nature Physics* **12**, 144-149, doi:10.1038/nphys3580 (2016).
- 8 Falson, J. *et al.* Type-II Ising pairing in few-layer stanene. *Science* **367**, 1454-1457, doi:10.1126/science.aax3873 (2020).
- 9 Bychkov, Y. A. & Rashba, E. I. Properties of a 2d Electron-Gas with Lifted Spectral Degeneracy. *Jetp Lett+* **39**, 78-81 (1984).
- 10 Liu, C. *et al.* Two-dimensional superconductivity and anisotropic transport at KTaO₃ (111) interfaces. *Science* **371**, 716-721, doi:10.1126/science.aba5511 (2021).
- 11 Chen, Z. *et al.* Two-Dimensional Superconductivity at the LaAlO₃/KTaO₃ (110) Heterointerface. *Physical Review Letters* **126**, 026802, doi:10.1103/PhysRevLett.126.026802 (2021).
- 12 Liu, C. *et al.* Tunable superconductivity and its origin at KTaO₃ interfaces. *Nature Communications* **14**, 951, doi:10.1038/s41467-023-36309-2 (2023).
- 13 Martínez, E. A., Dai, J., Tallarida, M., Nemes, N. M. & Bruno, F. Y. Anisotropic Electronic Structure of the 2D Electron Gas at the AlO_x/KTaO₃(110) Interface. *Adv. Electron. Mater.* **9**, 2300267, doi:10.1002/aelm.202300267 (2023).
- 14 Sugano, S., Tanabe, Y. & Kamimura, H. *Multiplets of Transition-Metal Ions in Crystals.* (Elsevier Science, 1970).
- 15 Al-Tawhid, A. H. *et al.* Enhanced Critical Field of Superconductivity at an Oxide Interface. *Nano Letters* **23**, 6944-6950, doi:10.1021/acs.nanolett.3c01571 (2023).
- 16 Singh, G. *et al.* Gap suppression at a Lifshitz transition in a multi-condensate superconductor. *Nature Materials* **18**, 948-954, doi:10.1038/s41563-019-0354-z (2019).
- 17 Annadi, A. *et al.* Anisotropic two-dimensional electron gas at the LaAlO₃/SrTiO₃ (110) interface. *Nature Communications* **4**, 1838, doi:10.1038/ncomms2804 (2013).
- 18 Wang, Z. *et al.* Anisotropic two-dimensional electron gas at SrTiO₃ (110). *Proc. Natl. Acad. Sci.* **111**, 3933-3937, doi:10.1073/pnas.1318304111 (2014).

- 19 Maki, K. & Tsuneto, T. Pauli Paramagnetism and Superconducting State. *Progress of Theoretical Physics* **31**, 945-956, doi:10.1143/ptp.31.945 (1964).
- 20 Tinkham, M. *Introduction to Superconductivity*. (Dover Publications, 2004).
- 21 Zhang, Z. *et al.* A spin-orbit scattering-enhanced high upper critical field at the LaAlO₃/KTaO₃(111) superconducting interface. *New Journal of Physics* **25**, 023023, doi:10.1088/1367-2630/acbae4 (2023).
- 22 Arnault, E. G. *et al.* Anisotropic superconductivity at KTaO₃ (111) interfaces. *Science Advances* **9**, eadf1414, doi:10.1126/sciadv.adf1414 (2023).
- 23 Werthamer, N. R., Helfand, E. & Hohenberg, P. C. Temperature and Purity Dependence of the Superconducting Critical Field, H_{c2}. III. Electron Spin and Spin-Orbit Effects. *Physical Review* **147**, 295-302, doi:10.1103/PhysRev.147.295 (1966).
- 24 Fischer, O., Decroux, M., Roth, S., Chevrel, R. & Sergent, M. Compensation of the paramagnetic effect on H_{c2} by magnetic moments: 700 kG superconductors. *Journal of Physics C: Solid State Physics* **8**, L474, doi:10.1088/0022-3719/8/21/014 (1975).
- 25 Xu, H. *et al.* Giant Tunability of Rashba Splitting at Cation-Exchanged Polar Oxide Interfaces by Selective Orbital Hybridization. *Advanced Materials* **36**, 2313297, doi:10.1002/adma.202313297 (2024).
- 26 Lama, B., Tsymbal, E. Y. & Paudel, T. R. Effects of intermixing and oxygen vacancies on a two-dimensional electron gas at the polar TbScO₃/KTaO₃ (001) interface. *Physical Review Materials* **7**, 026201, doi:10.1103/PhysRevMaterials.7.026201 (2023).
- 27 Klemm, R. A., Luther, A. & Beasley, M. R. Theory of Upper Critical-Field in Layered Superconductors. *Phys Rev B* **12**, 877-891, doi:10.1103/PhysRevB.12.877 (1975).
- 28 Fischer, O. H. Properties of High-Field Superconductors Containing Localized Magnetic Moments. *Helv. Phys. Acta* **45**, 331-397, doi:10.5169/seals-114388 (1972).
- 29 Balakirev, F. F. *et al.* Anisotropy reversal of the upper critical field at low temperatures and spin-locked superconductivity in K₂Cr₃As₃. *Phys Rev B* **91**, 220505, doi:10.1103/PhysRevB.91.220505 (2015).
- 30 Bao, J. K. *et al.* Superconductivity in Quasi-One-Dimensional K₂Cr₃As₃ with Significant Electron Correlations. *Phys Rev X* **5**, 011013, doi:10.1103/PhysRevX.5.011013 (2015).
- 31 Zuo, H. K. *et al.* Temperature and angular dependence of the upper critical field in K₂Cr₃As₃. *Phys Rev B* **95**, 014502, doi:10.1103/PhysRevB.95.014502 (2017).

- 32 Yang, J. *et al.* Spin-triplet superconductivity in $\text{K}_2\text{Cr}_3\text{As}_3$. *Sci Adv* **7**, eabl4432, doi:10.1126/sciadv.abl4432 (2021).
- 33 Silber, I. *et al.* Two-component nematic superconductivity in 4Hb-TaS_2 . *Nature Communications* **15**, 824, doi:10.1038/s41467-024-45169-3 (2024).
- 34 Hamill, A. *et al.* Two-fold symmetric superconductivity in few-layer NbSe_2 . *Nature Physics* **17**, 949-954, doi:10.1038/s41567-021-01219-x (2021).
- 35 Zhang, G. *et al.* Spontaneous rotational symmetry breaking in KTaO_3 heterointerface superconductors. *Nature Communications* **14**, 3046, doi:10.1038/s41467-023-38759-0 (2023).
- 36 Xie, Y. M., Zhou, B. T. & Law, K. T. Spin-Orbit-Parity-Coupled Superconductivity in Topological Monolayer WTe_2 . *Physical Review Letters* **125**, 107001, doi:10.1103/PhysRevLett.125.107001 (2020).
- 37 Cui, J. *et al.* Transport evidence of asymmetric spin-orbit coupling in few-layer superconducting $1\text{T}_d\text{-MoTe}_2$. *Nature Communications* **10**, 2044, doi:10.1038/s41467-019-09995-0 (2019).
- 38 Zhang, E. Z. *et al.* Spin-orbit-parity coupled superconductivity in atomically thin 2M-WS_2 . *Nature Physics* **19**, 106-113, doi:10.1038/s41567-022-01812-8 (2023).
- 39 Gan, Y. *et al.* Light-Induced Giant Rashba Spin–Orbit Coupling at Superconducting KTaO_3 (110) Heterointerfaces. *Advanced Materials* **35**, 2300582, doi:10.1002/adma.2023005820 (2023).
- 40 Al-Tawhid, A. H. *et al.* Superconductivity and Weak Anti-localization at KTaO_3 (111) Interfaces. *Journal of Electronic Materials* **51**, 6305-6309, doi:10.1007/s11664-022-09844-9 (2022).
- 41 Hua, X. *et al.* Tunable two-dimensional superconductivity and spin-orbit coupling at the $\text{EuO}/\text{KTaO}_3(110)$ interface. *npj Quantum Materials* **7**, 97, doi:10.1038/s41535-022-00506-x (2022).
- 42 Cai, X. *et al.* Disentangling spin-orbit coupling and local magnetism in a quasi-two-dimensional electron system. *Phys Rev B* **100**, 081402, doi:10.1103/PhysRevB.100.081402 (2019).

- 43 Maekawa, S. & Fukuyama, H. Magnetoresistance in Two-Dimensional Disordered Systems: Effects of Zeeman Splitting and Spin-Orbit Scattering. *Journal of the Physical Society of Japan* **50**, 2516-2524, doi:10.1143/JPSJ.50.2516 (1981).
- 44 Moetakef, P. *et al.* Carrier-Controlled Ferromagnetism in SrTiO₃. *Phys Rev X* **2**, 021014, doi:10.1103/PhysRevX.2.021014 (2012).
- 45 Dikin, D. A. *et al.* Coexistence of Superconductivity and Ferromagnetism in Two Dimensions. *Physical Review Letters* **107**, 056802, doi:10.1103/PhysRevLett.107.056802 (2011).
- 46 Wen, F. *et al.* Evolution of ferromagnetism in two-dimensional electron gas of LaTiO₃/SrTiO₃. *Applied Physics Letters* **112**, 122405, doi:10.1063/1.5009768 (2018).
- 47 Krantz, P. W., Tyner, A., Goswami, P. & Chandrasekhar, V. Intrinsic magnetism in KTaO₃ heterostructures. *Applied Physics Letters* **124**, 093102, doi:10.1063/5.0189956 (2024).
- 48 Hua, X. *et al.* Superconducting stripes induced by ferromagnetic proximity in an oxide heterostructure. *Nature Physics* **20**, 957-963, doi:10.1038/s41567-024-02443-x (2024).
- 49 Boon, M. R. Negative Magnetoresistance in Doped Semiconductors. *Phys Rev B* **7**, 761-762, doi:10.1103/PhysRevB.7.761 (1973).
- 50 Stamenov, P., Venkatesan, M., Dorneles, L. S., Maude, D. & Coey, J. M. D. Magnetoresistance of Co-doped ZnO thin films. *Journal of Applied Physics* **99**, 08M124, doi:10.1063/1.2172194 (2006).